Periodic spectral modulations of low-energy, low-charge-state carbon ions accelerated in an intense laser-solid interaction

Periodic spectral modulations of low-energy, low-charge-state carbon ions accelerated in an intense laser–solid interaction

Cite as: Phys. Plasmas **25**, 043122 (2018); https://doi.org/10.1063/1.5018596
Submitted: 07 December 2017 . Accepted: 27 March 2018 . Published Online: 27 April 2018

Muhammad Noaman-ul-Haq, Dong Wu, Hamad Ahmed, Boyuan Li, Xiaohui Yuan, Tongpu Yu, Xulei Ge, Thomas Sokollik, Liming Chen, Zhengming Sheng, and Jie Zhang

Periodic spectral modulations of low-energy, low-charge-state carbon ions accelerated in an intense laser–solid interaction

Muhammad Noaman-ul-Haq,[1,2,a)] Dong Wu,[3] Hamad Ahmed,[4] Boyuan Li,[1,2] Xiaohui Yuan,[1,2] Tongpu Yu,[5,6] Xulei Ge,[1,2,7] Thomas Sokollik,[1,2] Liming Chen,[1,2,8,b)] Zhengming Sheng,[1,2,6] and Jie Zhang[1,2]

[1]*Key Laboratory for Laser Plasmas (Ministry of Education), School of Physics and Astronomy, Shanghai Jiao Tong University, Shanghai 200240, China*
[2]*Collaborative Innovation Center of IFSA (CICIFSA), Shanghai Jiao Tong University, Shanghai 200240, China*
[3]*State Key Laboratory of High Field Laser Physics, Shanghai Institute of Optics and Fine Mechanics, 201800 Shanghai, China*
[4]*Centre for Plasma Physics, School of Mathematics and Physics, Queen's University Belfast, Belfast BT71NN, United Kingdom*
[5]*College of Science, National University of Defense Technology, Changsha 410073, China*
[6]*SUPA Department of Physics, University of Strathclyde, Glasgow G4 0NG, United Kingdom*
[7]*State Key Laboratory of Surface Physics and Department of Physics, Fudan University, Shanghai 200433, China*
[8]*Beijing National Laboratory of Condensed Matter Physics, Institute of Physics, CAS, Beijing 100190, China*

(Received 7 December 2017; accepted 27 March 2018; published online 27 April 2018)

We report experimental observation of periodic modulations in the energy distribution of C^{1+} ions dominantly accelerated in the interaction of a 15 μm thick tape target with intense laser pulses of intensities $\sim 10^{18}$ W/cm^2 in a defocused configuration. Moreover, the influence of laser intensity on the acceleration of low- and high-charge-state species of carbon ions is observed. Two-dimensional (2D) particle-in-cell simulations elucidate the dynamics of ionization-dependent acceleration of different species in different laser focusing conditions. By comparison, 1D simulations suggest that the modulations of C^{1+} ions are due to the longitudinal recirculation dynamics of hot electrons in the target, which modulates the sheath field for acceleration of C^{1+} ions. *Published by AIP Publishing.* https://doi.org/10.1063/1.5018596

I. INTRODUCTION

In the last few decades, laser-driven ion acceleration has been explored widely owing to its potential applications in medicine, materials processing, and high-energy physics.[1] One of the well-established and robust mechanisms for ion acceleration is target normal sheath acceleration (TNSA).[2] In this mechanism, hot electrons absorb laser energy and propagate through a target, causing the development of a strong sheath electric field (in the TV/m range) at the rear surface of the target due to charge separation. This field leads to ionization of atoms present at the rear surface, and consequently accelerates protons and other heavy ions such as carbon ions.[3] These accelerated ions exhibit unique properties, such as high brightness, short duration, and low emittance.[1] However, the typical spectrum of the ions is broadband with a sharp cutoff at the higher-energy end, rather than a mono-energetic spectral distribution, which is desirable for applications including cancer therapy.[4] Over the last decade, significant effort has been devoted to the control of the broad energy spread by tailoring laser and target parameters.[5–9] In addition, large modulations in the energy spectra have been reported in particular cases.[10–14] For instance, Clark *et al.*[10] observed modulations of protons and carbon ions as manifestations of a complex electron spectrum. Allen *et al.*[11] reported the presence of modulations in the proton spectrum due to multiple carbon ion species in the expanding plasma. Robinson *et al.*[12] found spectral modulations in the proton spectrum from nanometer-thick targets and related these to the magnetic field generated on the rear side of the target. Recently, using high-contrast ultrashort laser pulses, regular but faint modulations in the proton spectrum were reported, which were associated with pulsing electron beams having periodicity related to the half cycle of the laser field.[13] So far, no periodic modulations have been reported in heavy-ion spectra, which requires further investigation, as it is believed to be related to some regular phenomena on a relatively long time scale in ultra-intense laser–solid interaction.

In this paper, we report periodic modulations in the spectrum of low-energy C^{1+} ions by irradiating 15 μm-thick VHS (Video Home System) tape targets[15] with intense laser pulses. The data shows a significantly higher flux of low-charge-state carbon ions in the defocused configuration, which diminishes with increasing laser intensity and does not exhibit periodic oscillations in the spectra. Moreover, closer to the best focus, high-charge-state carbon ions (C^{4+}) and protons to higher energies are observed. These observations are considered as laser-intensity-dependent ionization dynamics of carbon ion species. Two-dimensional (2D) particle-in-cell (PIC) simulations also corroborate intensity-dependent acceleration of different charge states of carbon ions. In addition, 1D simulations have been performed by considering the planar

a)haq.noaman@sjtu.edu.cn
b)lmchen@iphy.ac.cn

plasma expansion in quasi one dimension.[16] In the simulations, recirculating hot electrons have been observed on time scales longer than the incident laser pulse duration. The dynamics of the recirculating hot electrons are more likely responsible for the modulations seen on the time-integrated raw traces of C^{1+} ions. These observations could be helpful in the development of a dynamic representation of the TNSA mechanism incorporating recirculation dynamics of the hot electrons.[17,18]

II. EXPERIMENTAL SETUP

The experiment was carried out at the Laboratory for Laser Plasmas (LLP), Shanghai Jiao Tong University. A Ti: sapphire-based laser system was used, which can deliver *p*-polarized pulses of ∼25 fs duration and maximum energy of ∼5 J at 10 Hz repetition rate. In this work, the laser pulse energy was ∼1.5 J on the target. The contrast of the amplified spontaneous emission (ASE) to the main peak was measured to be 10^{-8} at 10 ps using a scanning third-order autocorrelator (Sequoia).[19] Fig. 1 shows a schematic of the experimental setup. Laser pulses of ∼30 fs duration were focused to ∼6 μm spot (full width at half maximum, FWHM) at ∼54°, using an *f*/4 off-axis parabolic mirror (OAP), containing 25% of the energy in the FWHM. The resulting peak intensity was $\sim 5 \times 10^{19}$ W/cm^2. A tape-drive target system with VHS tape of thickness 15 μm was employed, which was mounted on a motorized 3D translation stage system. Such a tape-drive target system can be used for numerous laser shots at a high repetition rate without frequent opening of the target chamber. The VHS tape used is composed of magnetic iron oxide (1.5 μm) and Mylar substrate (13.5 μm), which has already been used for the generation of higher-order harmonics,[20] plasma mirrors,[21] and ion acceleration.[15] In the experiment, the laser intensity on the target was varied by moving the target in the upstream direction (toward the OAP) using the precise motorized stages with a resolution of 0.2 μm. A Thomson parabola spectrometer (TPS) was installed along the target normal direction. It consists of a magnet with an effective field strength of ∼0.33 T and a gap of 25 mm between the poles. Copper electrode plates with a voltage difference of ∼4 kV were fitted on the poles for compactness of the system. An adjustable slit[13] of width ranging from 70 to 220 μm and length 3 mm oriented along the *x* axis was installed at a distance of ∼755 mm from the target at the entrance of the TPS. The spectrometer could collect the ions emitted between angles of ∼4 and ∼93 μrad in the horizontal and vertical directions, respectively, subtending a solid angle of $\sim 1.86 \times 10^{-7}$ sr. The energy resolution of the spectrometer was 2%–4% for the carbon ions. The ion traces were recorded using a microchannel plate (MCP) detector of diameter 40 mm equipped with a 14-bit CCD camera (Point Grey).

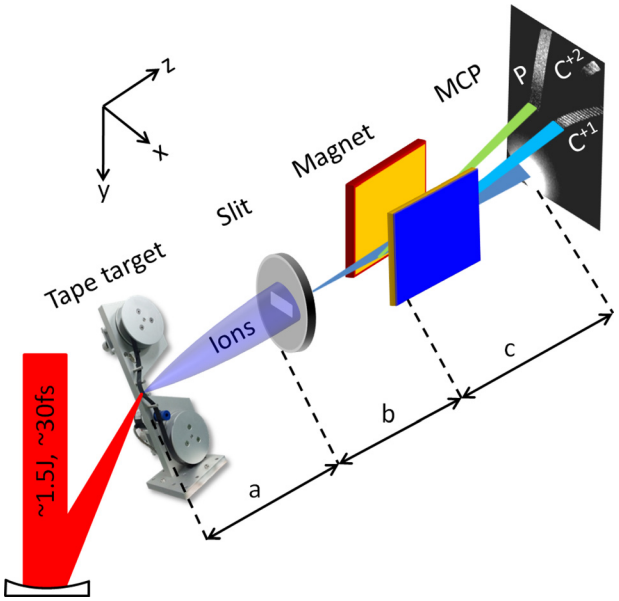

FIG. 1. Schematic of the experimental setup for ion acceleration in the interaction of intense laser pulses with a VHS tape-drive target system. The distances *a*, *b*, and *c* are 75.5, 11.05, and 22.4 cm, respectively. The electric and magnetic fields in the spectrometer are along the *x* axis.

III. EXPERIMENTAL RESULTS

Figures 2(a)–2(f) show ion traces on the MCP detector with the laser intensity varying as the target is moved toward the OAP. The corresponding laser intensities were calculated using the focal spot sizes obtained at low energies as shown in Fig. 2(g). As can be seen in Fig. 2(a), at the best focus, an almost pure proton beam is observed, with significantly lower counts of carbon ions. Since the ionization potential for protons is lower and their charge-to-mass ratio is higher, these are accelerated more effectively. Also, this could screen the sheath field to accelerate the relatively heavier ions.[3] As the laser intensity is varied by moving the target, the proton energy decreases with little increase in the counts for low energy; in addition, C^{4+} ions become more visible, as shown in Fig. 2(b). A further decrease in laser intensity leads to increased visibility of low-charge-state carbon ions, since the strength of the sheath electric field required for acceleration of the higher charge states decreases, although it is still strong enough for the low-charge-state carbon ions, as shown in Fig. 2(c). Moreover, high-charge-state carbon species disappear for target positioning at 360 μm or further away, whereas large counts for low-charge-state carbon ions are observed as shown in Figs. 2(d)–2(f) for further variations in the corresponding sheath field. Interestingly, clear spectral modulations appear in the C^{1+} ions, with an obvious contrast with the background. Figure 2(e) shows the modulations of the C^{1+} ions with the most distinct contrast. Energy spectra of protons and carbon ions for the focused and defocused configurations are shown in Figs. 2(h) and 2(i), respectively. The proton spectrum shows a few dips and peaks, which can be attributed to multispecies acceleration as described in Ref. 22; however, no regular modulations are observed. These irregular modulations are beyond the scope of this work. The maximum energy of the protons is ∼7.5 MeV, as shown in Fig. 2(h), and the energy drops to ∼3 MeV for the defocused configuration. The energy of the C^{1+} ions is 300 keV, an order of magnitude lower than that of the protons. However, the counts for C^{1+} ions are an order of magnitude higher than those for protons. The energy spectrum of C^{1+} ions shows clear periodic wiggles, with the

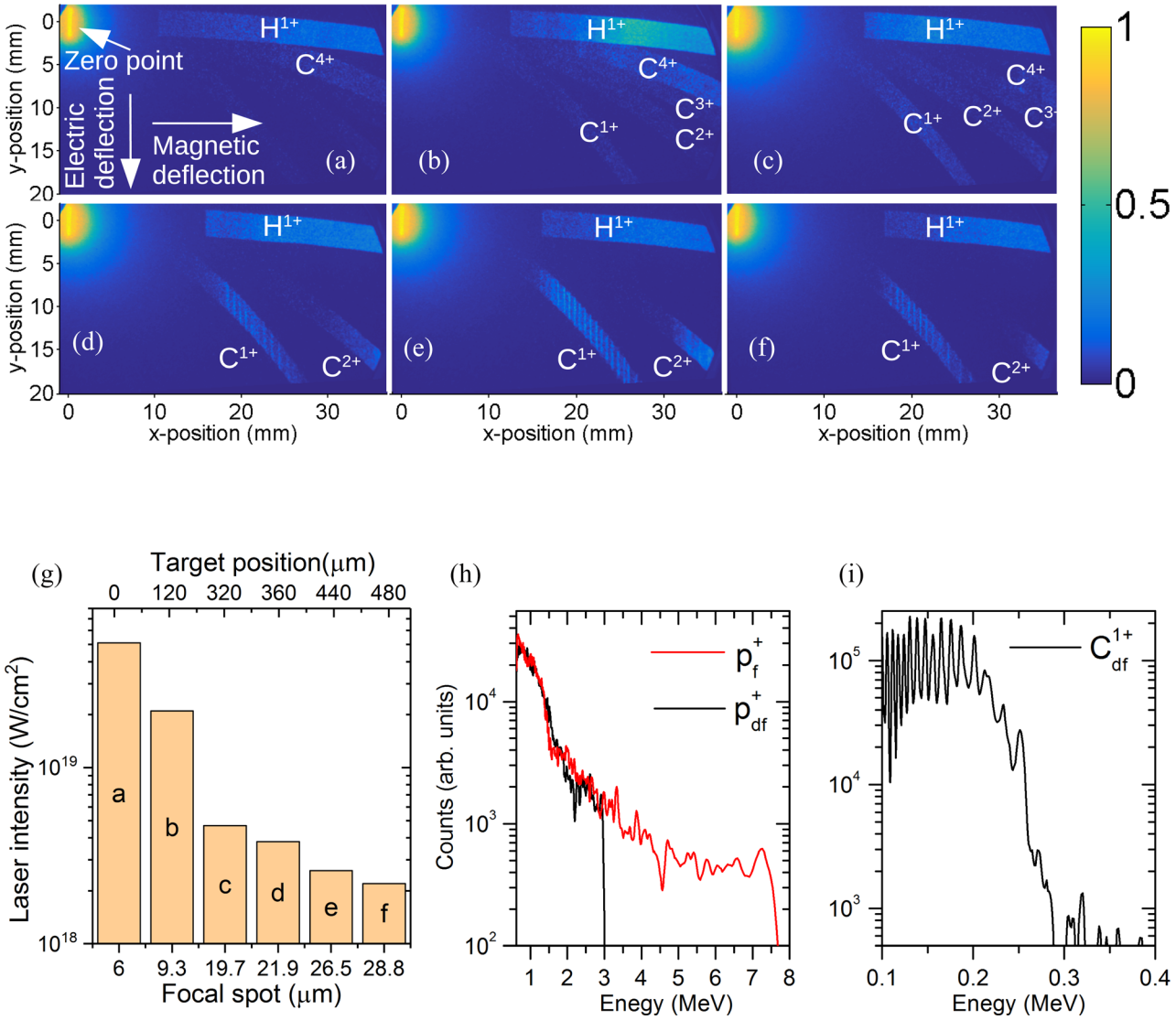

FIG. 2. Raw ion traces on the MCP detector. (a)–(f) Variation of ion traces and (d)–(f) appearance of modulations on C^{1+} with decreasing intensity as the target is moved before the best focus (toward the OAP). (g) Laser intensity and focal spot on the target as a function of the target position for (a)–(f). (h)–(i) Energy spectra for protons and C^{1+} ions for focus (subscript "f") and defocus (subscript "df") extracted from (a) and (e).

spacing between peaks becoming larger toward the higher-energy part of the spectrum, showing a chirped effect. Such peaks are not found in the proton spectrum in the entire range of intensity, no matter whether this is higher or lower. To confirm the presence of modulations in the C^{1+} ions as a physical phenomenon, precise target scans were carried out for numerous laser shots, and a modulated pattern was reproducible in the C^{1+} ions similar to that shown in Figs. 2(d)–2(f). It is important to note that, as far as we know, this is the first reported observation of regular and reproducible periodic modulations in C^{1+} ions.

IV. PARTICLE-IN-CELL SIMULATIONS AND DISCUSSION

Two main observations can be noted in Fig. 2. One is the acceleration of different states of carbon ions as the laser intensity changes, and the other is the presence of prominent periodic modulations in the C^{1+} ions. In order to confirm the influence of laser intensity on ionization of carbon species, for both focused and defocused configurations, we carried out 2D numerical simulations using the PIC program LAPINE,[23] which includes both ionization and collision dynamics.[24,25] In the simulations, the laser wavelength was taken as 0.8 μm. The dimensionless maximum amplitude of the laser electric field was taken as $a_0 = 5$ for the intensity at tight focus and $a_0 = 1$ for the intensity in the defocused configuration. However, the beam spot radius was chosen as 5 μm in both configurations, with an incident angle of 54°. The target configuration was taken to be almost the same as that used in the experiment, with 1.5 μm iron and 13.5 μm plastic material. The iron density was 7.9 g/cm^3, the corresponding iron atom density was $n_{Fe} = 80n_c$ (where n_c is the plasma critical density), the plastic (C: H = 1: 1) density was 1 g/cm^3, and the corresponding carbon (hydrogen) density was $n_C = 40n_c$ ($n_H = 40n_c$). The initial charge state of iron was 4+, while the plastic was considered to be an insulator without any free electrons.

Figure 3 shows the results of the simulation of the laser intensity for the two different configurations. For a relatively tight focus, the laser intensity is higher Figs. 3(a)–3(d)], the

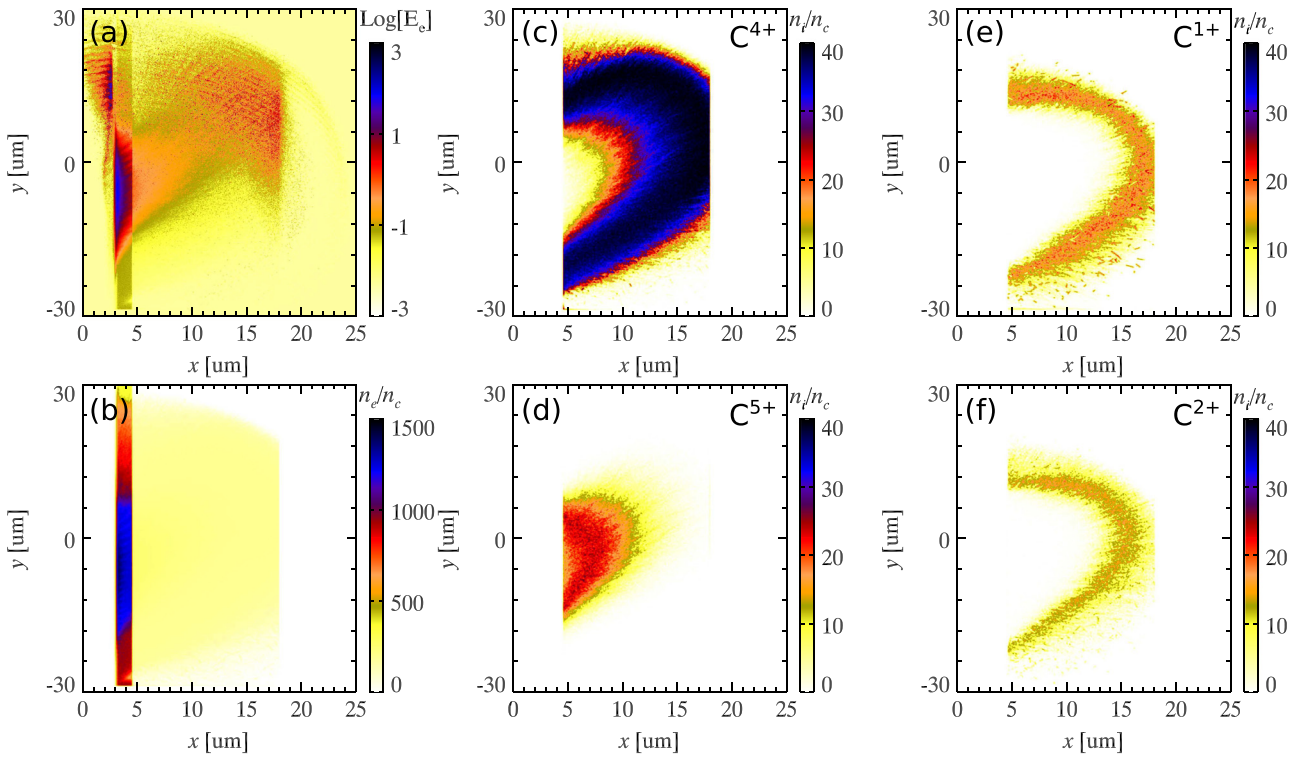

FIG. 3. Two-dimensional simulation results. For a laser amplitude $a_0 = 5$, (a)–(d) show the electron energy density distribution, the free-electron density distribution, and the C^{4+} and C^{5+} density distributions at $t = 35T$. For a laser amplitude $a_0 = 1$, (e) and (f) show the corresponding C^{1+} and C^{2+} density distributions at $t = 35T$.

hot electrons produced in front of the tape will significantly ionize the remainder of the target, and the majority of the carbon is ionized to C^{4+}. For a defocused beam, the effect of the laser intensity is weaker, the ionization of the target is not efficient, and therefore, only low-charge-state carbon ions can be produced, as shown in Figs. 3(e) and 3(f). In this paper, we do not intend to classify the different ionization mechanisms (field ionization or collisional ionization): our 2D simulations are used to show the dependence of the ionization charge states on laser intensities. These results are also consistent with reported observations for intensity-dependent ionization/acceleration of carbon ion species for planar targets in Ref. 26. In addition, we noticed the existence of double-frequency electron bunches resulting from $j \times B$ heating in our simulations, which may lead to regular modulations of the ions.[13] We performed an analysis similar to that in Ref. 13 for the spectrum of protons in Fig. 2(h) to observe the maxima and minima of the modulations; however, no regular pattern of modulations could be observed. Moreover, the model presented in Ref. 13, originally for regular modulations on single ion species (protons) linked to double-frequency electrons, and requiring a very large temporal parameter, is not found to be consistent with the regular modulations of C^{1+} ions in our case. In this context, for thicker targets, owing to the persistence of the electron recirculation phenomenon on longer time scales[27] and the longer response time of C^{1+} ions, we propose a link between regular modulations of C^{1+} and electron recirculation dynamics.

In order to understand the observation of modulations of C^{1+} ions in the defocused configuration, we performed 1D3V PIC simulations using the code OSIRIS.[28] Since the laser pulse length ($L_p = c\tau_p$) in our experiment was $\sim 9\,\mu$m (FWHM), in the tight-focus case, the focal spot size is very close to the pulse length. Therefore, the laser will cause a strong nonuniform force in the laser–plasma interaction due to a transversely nonflat intensity distribution. However, when the laser is defocused and the area of laser intensity is far larger than the pulse length, the effect of transverse nonuniformity will be removed and the laser–plasma interaction can be treated as quasi-1D. The simulation region was taken to be $120\,\mu$m long and to consist of 8000 cells. The total run time was $700T_0$, where $T_0 = 3.3$ fs. Initially, a cold and uniform target was positioned at $50\,\mu\text{m} \le x \le 65\,\mu$m. The target was considered to be a fully ionized plasma of density $n_e = 60n_c$, and the ion species were taken to be C^{1+} and protons with equal densities. It is worth mentioning that, based on our 2D simulation results showing the influence of laser intensity on carbon ions, we considered only dominant C^{1+} ions with protons. In the simulations, 10 000 macroparticles per cell were allocated to the plasma region. A linearly polarized laser with $a_0 = 5$ propagated in the positive x direction toward the target. The pulse duration was $\sim$30 fs. The laser intensity in the simulations was kept high, in order to simulate the main stage of the interaction qualitatively, without consideration of the prepulse and pre-plasma (and many other effects). Since the contrast of the laser pulses in the experiment was relatively low, for the thicker target the scale length of the pre-plasma might be large enough[29] to significantly enhance the laser absorption. This can increase the electron density, in addition to the increase in density due to oblique incidence. Therefore, we chose the value of a_0 in the 1D simulations such that the maximum proton energy was

comparable to the experimental results shown in Fig. 2(h) for the defocused configuration. As ion acceleration in TNSA is due to the sheath field developed as the hot electrons cross the rear side of the target, we observed trajectories of 200 random hot electrons with 1 fs time steps. Tracks for a typical electron are shown in Fig. 4(a). A clear recirculation of electrons can be seen with our simulation parameters, with five round trips about the 15 μm-thick target. The starting position is near the front surface of the target. The electron momentum decreases in each round trip, indicating deceleration. In addition to spatial variations, the temporal variations in the momentum of the electron are also shown in Fig. 4(b). The momentum is initially high, but then decreases, with an overall damped oscillatory behavior. Also, from the third track, we can see that the spacing between peaks is increasing, since the decelerating electrons take longer to complete the round trip. This indicates some kind of chirp effect, which is not well fitted with the damped sine function from the fourth round trip, as shown in Fig. 4(b). However, we believe that this deceleration and chirp effect could be linked with the chirpiness shown in Fig. 2(e). It is worth mentioning that such effects have also been reported for modulations on protons in Ref. 13. Since modulations are likely to be an intrinsic property of laser-driven ions, this phenomenon may be attributed to one of their characteristics.

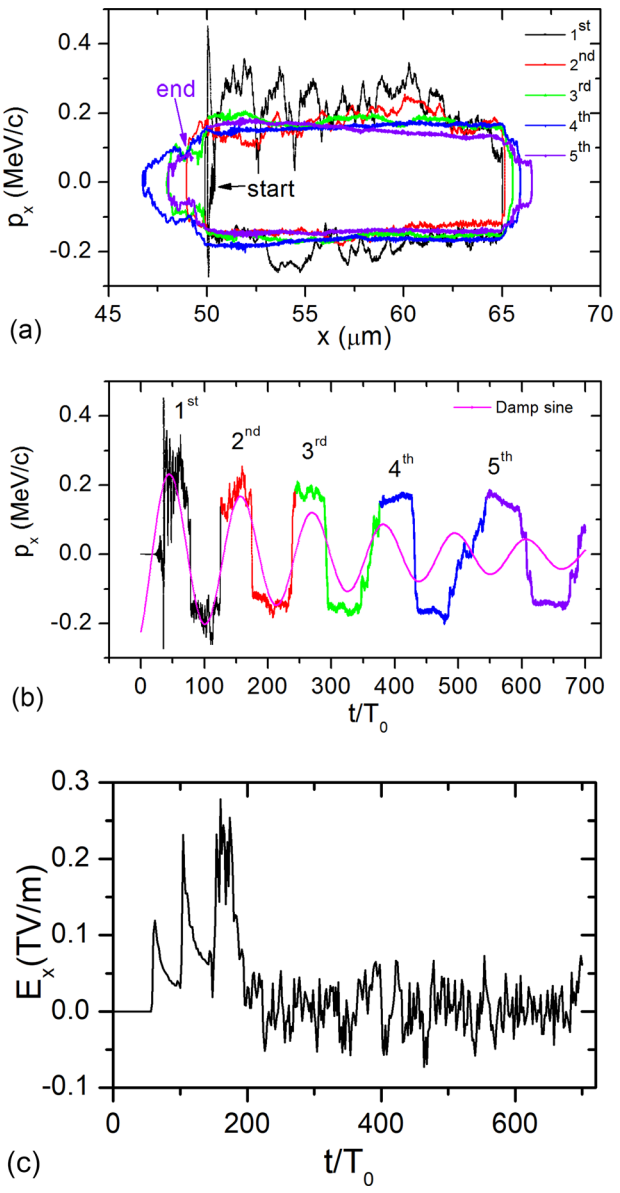

FIG. 4. Example of the recirculation of the hot electrons in the simulations. (a) Tracking of a typical electron in momentum space. (b) Temporal evolution of the momentum of the same electron. The legends in (a) denote the round-trip numbers. (c) Typical example of the evolution of the E_x field 2 μm away from the rear of the target.

In addition to recirculation, in the simulation, electrons escaping from the rear of the target were also observed (not shown here). The recirculation and escape of electrons indicate a varying density distribution of hot electrons[18] on the rear of the target, which strongly affects the sheath field. Figure 4(c) shows a typical example of the temporal evolution of the sheath field observed 2 μm from the rear of the target. Similar variations are observed at greater distances. Since the carbon ions can be regarded as tracers giving information about the accelerating field,[3,30,31] the results strongly indicate the effect of the modulated sheath field on C^{1+} ions in our experiment. Simulated C^{1+} and proton energy spectra are shown in Fig. 5. The presence of modulated peaks is very clear in the C^{1+} spectrum. Although the simulation results do not exactly reproduce the experimental results extracted from time-integrated raw data on the detector, they clearly show the modulated peaks in the C^{1+} spectrum. In addition, the modulation period (in energy) becomes larger for higher-energy C^{1+} ions in the spectrum. As can be seen in Fig. 5(b), the proton spectrum does not show any prominent modulations. These features are qualitatively consistent with the experimental results shown in Fig. 2(e) and indicate that the recirculation of hot electrons could affect the acceleration of C^{1+} ions.

The experimental data suggest that modulations are observed in low-charge-state carbon ions (C^{1+}), in addition to the variation of carbon ion species with laser intensity. The dependence of the modulations on the ion species could be related to the sheath field dynamics as described in Refs. 31 and 32. In those works, the spatio-temporal distribution of the sheath field and the acceleration dynamics at the rear side of the target were deduced from the spectra of the carbon ions. Moreover, Hegelich *et al.*[32] discussed the strength

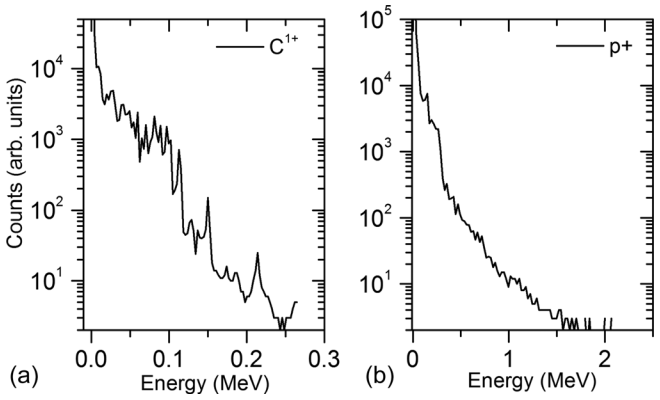

FIG. 5. Simulated C^{1+} (a) and proton (b) energy spectra at $t = 700T_0$.

of the sheath field and acceleration time and length of different carbon ion species. For instance, the maximum sheath field for C^{1+} ions is two orders of magnitude lower than for higher-charge-state ions (C^{4+}), but has a greater acceleration time and length.[32] In the work presented here, it is very likely that these low-charge-state ions are observed particularly in the defocused configuration because the relatively weak sheath field is only sufficient for lower ionization states. In contrast, owing to their greater acceleration time and length,[30,32] the modulations in their spectra become more pronounced. As can be seen in Fig. 2(e), weak modulation features are also seen in C^{2+}, but are not as clearly visible as in C^{1+}. For higher charge states of carbon ions, the acceleration time and length are shorter (by about two orders of magnitude),[30,32] and therefore, the modulations are likely to be weak. It is important to note that although the above explanations seem plausible, further detailed simulations are required, incorporating larger focal spot sizes and sheath field ionization effects.

V. CONCLUSIONS

We have presented experimental results on the ionization-dependent acceleration of carbon ion species in the interaction of an intense laser with a solid target. The data clearly shows that acceleration of higher-charge-state carbon ions is evident at higher laser intensity (a tight focus), while in the defocused configuration, the acceleration of C^{1+} is dominant, with pronounced periodic modulations at the lower end of the spectrum. Supporting 2D PIC simulations illustrate the interplay of different laser absorption mechanisms with the laser intensity variations at different laser focusing configurations. The observation of modulations of C^{1+} ions is explained by 1D PIC simulations, which indicate the role of longitudinal recirculation of the hot electrons in the spatial and temporal evolution of the sheath field. The relatively slow response of C^{1+} ions to the varying sheath field results in modulations of the C^{1+} spectrum. Moreover, in comparison with previously reported modulations of protons,[13] there is a signature of chirp in the spectral modulations of C^{1+}, which could be attributed to deceleration of recirculating hot electrons and the corresponding evolution of the sheath field. These results may be helpful in further studies to provide a dynamical description of the TNSA mechanism, incorporating the role of recirculation dynamics of the hot electrons[17,18] to completely understand the modulations.

ACKNOWLEDGMENTS

We acknowledge fruitful discussions with Noureddine Oudini and Matthias Schnürer. We would also like to acknowledge the OSIRIS Consortium, consisting of UCLA and IST (Lisbon, Portugal) for the use of OSIRIS and the visXD framework. This work was supported by the National Basic Research Program of China (under Grant No. 2013CBA01500), the National Natural Science Foundation of China (under Grant Nos. 11421064, 11475113, 11605269, and 11622547), and the Science Challenge Project (under Grant No. TZ2016005). The data associated to the results presented in this article can be accessed by contacting the corresponding authors.

[1]A. Macchi, M. Borghesi, and M. Passoni, Rev. Mod. Phys. **85**, 751 (2013).
[2]S. C. Wilks, A. B. Langdon, T. E. Cowan, M. Roth, M. Singh, S. Hatchett, M. H. Key, D. Pennington, A. MacKinnon, and R. A. Snavely, Phys. Plasmas **8**, 542 (2001).
[3]M. Hegelich, S. Karsch, G. Pretzler, D. Habs, K. Witte, W. Guenther, M. Allen, A. Blazevic, J. Fuchs, J. C. Gauthier, M. Geissel, P. Audebert, T. Cowan, and M. Roth, Phys. Rev. Lett. **89**, 085002 (2002).
[4]L. N. Su, Z. D. Hu, Y. Zheng, M. Liu, Y. T. Li, W. M. Wang, Z. M. Sheng, X. H. Yuan, M. H. Xu, Z. W. Shen, H. T. Fan, L. M. Chen, X. Lu, J. L. Ma, X. Wang, Z. H. Wang, Z. Y. Wei, and J. Zhang, Phys. Plasmas **21**, 093111 (2014).
[5]B. M. Hegelich, B. J. Albright, J. Cobble, K. Flippo, S. Letzring, M. Paffett, H. Ruhl, J. Schreiber, R. K. Schulze, and J. C. Fernández, Nature **439**, 441 (2006).
[6]H. Schwoerer, S. Pfotenhauer, O. Jackel, K.-U. Amthor, B. Liesfeld, W. Ziegler, R. Sauerbrey, K. W. D. Ledingham, and T. Esirkepov, Nature **439**, 445 (2006).
[7]C. Brabetz, S. Busold, T. Cowan, O. Deppert, D. Jahn, O. Kester, M. Roth, D. Schumacher, and V. Bagnoud, Phys. Plasmas **22**, 013105 (2015).
[8]E. d'Humières, A. Brantov, V. Y. Bychenkov, and V. T. Tikhonchuk, Phys. Plasmas **20**, 023103 (2013).
[9]S. S. Bulanov, C. B. Schroeder, E. Esarey, and W. P. Leemans, Phys. Plasmas **19**, 093112 (2012).
[10]E. L. Clark, K. Krushelnick, M. Zepf, F. N. Beg, M. Tatarakis, A. Machacek, M. I. K. Santala, I. Watts, P. A. Norreys, and A. E. Dangor, Phys. Rev. Lett. **85**, 1654 (2000).
[11]M. Allen, Y. Sentoku, P. Audebert, A. Blazevic, T. Cowan, J. Fuchs, J. C. Gauthier, M. Geissel, M. Hegelich, S. Karsch, E. Morse, P. K. Patel, and M. Roth, Phys. Plasmas **10**, 3283 (2003).
[12]A. P. L. Robinson, P. Foster, D. Adams, D. C. Carroll, B. Dromey, S. Hawkes, S. Kar, Y. T. Li, K. Markey, P. McKenna, C. Spindloe, M. Streeter, C.-G. Wahlström, M. H. Xu, M. Zepf, and D. Neely, New J. Phys. **11**, 083018 (2009).
[13]M. Schnürer, A. A. Andreev, F. Abicht, J. Bränzel, C. Koschitzki, K. Y. Platonov, G. Priebe, and W. Sandner, Phys. Plasmas **20**, 103102 (2013).
[14]F. Sylla, "Ion acceleration from laser–plasma interaction in underdense to near-critical Regime: Wakefield effects and associated plasma structures," Ph.D. thesis (Ecole Polytechnique X, 2011).
[15]M. Noaman-ul Haq, H. Ahmed, T. Sokollik, L. Yu, Z. Liu, X. Yuan, F. Yuan, M. Mirzaie, X. Ge, L. Chen, and J. Zhang, Phys. Rev. Accel. Beams **20**, 041301 (2017).
[16]A. Yogo, K. Mima, N. Iwata, S. Tosaki, A. Morace, Y. Arikawa, S. Fujioka, T. Johzaki, Y. Sentoku, H. Nishimura, A. Sagisaka, K. Matsuo, N. Kamitsukasa, S. Kojima, H. Nagatomo, M. Nakai, H. Shiraga, M. Murakami, S. Tokita, J. Kawanaka, N. Miyanaga, K. Yamanoi, T. Norimatsu, H. Sakagami, S. V. Bulanov, K. Kondo, and H. Azechi, Sci. Rep. **7**, 42451 (2017).
[17]M. Passoni, C. Perego, A. Sgattoni, and D. Batani, Phys. Plasmas **20**, 060701 (2013).
[18]C. Perego, "Target normal sheath acceleration for laser-driven ion generation: Advances in theoretical modeling," Ph.D. thesis (Universitá degli Studi Milano-Bicocca, Milan, Italy, 2013).
[19]Y. Fang, T. Yu, X. Ge, S. Yang, W. Wei, T. Yuan, F. Liu, M. Chen, J. Liu, Y. Li, X. Yuan, Z. Sheng, and J. Zhang, Plasma Phys. Controlled Fusion **58**, 045025 (2016).
[20]B. H. Shaw, J. van Tilborg, T. Sokollik, C. B. Schroeder, W. R. McKinney, N. A. Artemiev, V. V. Yashchuk, E. M. Gullikson, and W. P. Leemans, J. Appl. Phys. **114**, 043106 (2013).
[21]S. Steinke, J. van Tilborg, C. Benedetti, C. G. R. Geddes, C. B. Schroeder, J. Daniels, K. K. Swanson, A. J. Gonsalves, K. Nakamura, N. H. Matlis, B. H. Shaw, E. Esarey, and W. P. Leemans, Nature **530**, 190 (2016).
[22]A. J. Kemp and H. Ruhl, Phys. Plasmas **12**, 033105 (2005).
[23]H. Xu, W. W. Chang, H. B. Zhuo, L. H. Cao, and Y. Z. W. Chin, J. Comput. Phys. **19**, 305 (2002).
[24]D. Wu, X. T. He, W. Yu, and S. Fritzsche, Phys. Rev. E **95**, 023208 (2017).
[25]D. Wu, X. T. He, W. Yu, and S. Fritzsche, Phys. Rev. E **95**, 023207 (2017).
[26]M. Schnürer, S. Ter-Avetisyan, P. V. Nickles, and A. A. Andreev, Phys. Plasmas **14**, 033101 (2007).
[27]Y. Sentoku, T. E. Cowan, A. Kemp, and H. Ruhl, Phys. Plasmas **10**, 2009 (2003).

[28]R. A. Fonseca, L. O. Silva, F. S. Tsung, V. K. Decyk, W. Lu, C. Ren, W. B. Mori, S. Deng, S. Lee, T. Katsouleas, and J. C. Adam, in *Computational Science—ICCS 2002: International Conference Amsterdam, The Netherlands, April 21–24, 2002 Proceedings, Part III* (Springer, Berlin, 2002).
[29]H. Daido, M. Nishiuchi, and A. S. Pirozhkov, Rep. Prog. Phys. **75**, 056401 (2012).
[30]P. McKenna, D. C. Carroll, R. J. Clarke, R. G. Evans, K. W. D. Ledingham, F. Lindau, O. Lundh, T. McCanny, D. Neely, A. P. L. Robinson, L. Robson, P. T. Simpson, C.-G. Wahlström, and M. Zepf, Phys. Rev. Lett. **98**, 145001 (2007).
[31]J. Schreiber, M. Kaluza, F. Grüner, U. Schramm, B. Hegelich, J. Cobble, M. Geissler, E. Brambrink, J. Fuchs, P. Audebert, D. Habs, and K. Witte, Appl. Phys. B **79**, 1041 (2004).
[32]B. M. Hegelich, "Acceleration of heavy ions to Mev/nucleon energies by ultrahigh-intensity lasers," Ph.D. thesis (Ludwig-Maximilians-Universität München, 2002).